Investigation of drain noise in InP pHEMTs using cryogenic on-wafer characterization

Bekari Gabritchidze^{#1}, Kieran Cleary^{#2}, Anthony Readhead[#], Austin J. Minnich^{*3}

*Cahill Radio Astronomy Lab, California Institute of Technology, USA

*Division of Engineering and Applied Science, California Institute of Technology, USA

¹bekari@caltech.edu, ²kcleary@astro.caltech.edu, ³aminnich@caltech.edu

Abstract — We present on-wafer measurements of microwave noise temperature and S-parameters of InP pseudomorphic high electron mobility transistors (pHEMTs) over various drain-source voltages (V_{DS}) and physical temperatures (T_{ph}) . From these data, we extract the small signal model (SSM) and drain noise temperature T_d at each V_{DS} and T_{ph} . We find that T_d follows a non-linear trend with both V_{DS} and T_{ph} . The observed trends are consistent with a recent drain noise model [1], [2], where T_d originates from the sum of a thermal noise, attributed to physical temperature of electrons (T_{el}) in the channel; and real-space transfer (RST) noise, attributed to thermionic emission of electrons from the channel to the barrier. Using this model, we find that at the bias that minimizes the noise temperature, RST accounts for $\sim 50\%$ of T_d at 300 K and $\sim 30\%$ at 40 K. Possible improvements in noise performance in pHEMTs if RST were suppressed are discussed.

Keywords — Cryogenics, drain noise, InP HEMTs, Low noise amplifiers, real-space transfer

I. INTRODUCTION

High electron mobility transistors based on InP are widely used in low noise amplifiers operating in the microwave and millimeter-wave frequencies [3], [4], [5], [6], [7], [8]. Despite their widespread adoption and record microwave noise performance [5], [9], the physical mechanism of the dominating noise source, drain noise, is still a topic of investigation [10], [2], [11]. Prior explanations for drain noise include the suppressed shot noise theory [10], [12]. The theory makes predictions such as a temperature-independent output noise power, but other works have found the predictions to be inconsistent with experimental observations [11], [1], [13]. Recently, a physical model of drain noise was proposed [1] in which drain noise was attributed to a thermal component associated to the physical temperature of electrons (T_{el}) in the channel and a component due to RST of electrons from the channel to the barrier (T_{RST}) [2]. This model was able to account for the observed dependence of T_d on V_{DS} and T_{ph} for GaAs mHEMTs. [1]

In this paper, we extend the characterization of T_d reported previously for GaAs mHEMTs [13] to InP pHEMTs. We present the on-wafer characterization of the microwave noise (T_{50}) at a generator impedance of 50 Ω and S-parameters of InP pHEMTs over a range of V_{DS} and T_{ph} . From the data, we develop SSM and noise models that yield T_d at each V_{DS} and T_{ph} . We find that T_d exhibits a nonlinear dependence on V_{DS} and T_{ph} , with the trends being consistent with those reported for GaAs mHEMTs [1]. Using the model, we find that, at the

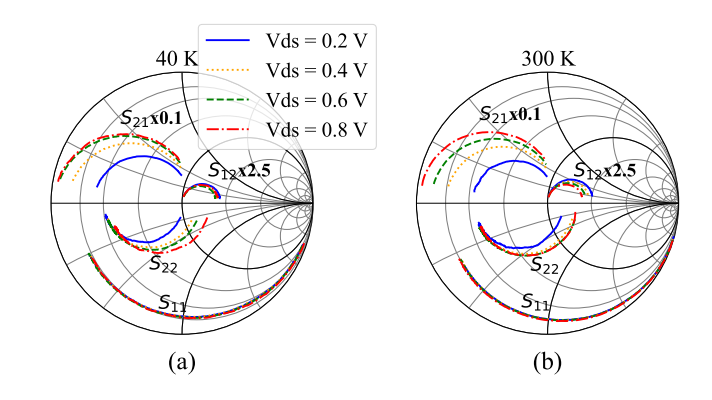


Fig. 1. S-parameters measurements of InP pHEMTs from 1-18 GHz for V_{DS} in the range 0.2-0.8 V, at $T_{ph}=40~{\rm K}$ (a) and $T_{ph}=300~{\rm K}$ (b). V_{GS} was kept constant at 12.9 mV (a) and -10 mV (b).

bias which minimizes T_{50} , RST accounts for ~ 30 % of T_d at $T_{ph}=40$ K and ~ 50 % at $T_{ph}=300$ K. The model indicates that a suppression of RST noise, for example by improving the electron confinement in the quantum well, could lead to the reduction of minimum noise temperature (T_{min}) by $\sim 25\%$ and $\sim 15\%$ at 300 K and 40 K, respectively.

II. DEVICE CHARACTERIZATION AND MODELLING

The S-parameters and the microwave noise of InP pHEMTs (Diramics, pH-100, 4F50, gate length $L_q = 100$ nm) were measured using a cryogenic probe station (CPS) similar to [13]. A hybrid SSM extraction was used. First, the parasitics were determined from open and short structure characterization [14]. The parasitic gate resistances (R_q) provided by the manufacturer at 15 K and 300 K were used, as it was not possible to extract the values from the open/short structures. The R_g at intermediate T_{ph} were determined by linear interpolation of the provided values. After de-embedding the parasitics, the intrinsic parameters were determined through direct extraction and then optimization in Keysight ADS following [13], [15], [14], [16]. Once the SSM was established, T_d was determined by fitting the measured and modeled T_{50} [17], [18], [13]. The modelled noise parameters were extracted automatically with Keysight ADS from the SSM and noise models.

III. EXPERIMENTAL RESULTS

The S-parameters of discrete InP pHEMTs were measured on-wafer over a range of V_{DS} from $0.1-0.8~{\rm V}$ and constant V_{GS} of 12.9 mV and -10 mV at 40 K and 300 K, respectively. The V_{GS} were selected so that at $V_{DS}=0.8~{\rm V}$, the difference between V_{GS} and threshold voltage (V_{th}) was 94 mV, following the study for the GaAs mHEMTs [1]. Fig. 1 shows the measured S-parameter at 40 K (Fig. 1a) and 300 K (Fig. 1b). At a given T_{ph} , S_{21} and S_{22} exhibit a clear variation with V_{DS} while S_{11} and S_{12} show a smaller but observable dependence.

Figs. 2a and 2b show the small signal transconductance (g_m) and drain conductance (g_{ds}) versus V_{DS} at 40 K and 300 K, respectively. g_m increases with V_{DS} at both T_{ph} , however, at 40 K and $V_{DS}=0.5$ V, a maximum of $\sim 1200~{\rm mS\cdot mm^{-1}}$ is achieved. At higher V_{DS} , a decrease of $\sim 200~{\rm mS\cdot mm^{-1}}$ is observed. g_{ds} decreases with increasing V_{DS} at each T_{ph} but plateaus for $V_{DS}\gtrsim 0.4$ V and $T_{ph}=300$ K. In Fig. 2c, g_m and g_{ds} are plotted versus T_{ph} at constant $V_{DS}=0.6$ V and $I_{DS}=10$ mA. Both quantities are observed to decrease with increasing T_{ph} . Similar values and trends of g_m and g_{ds} with V_{DS} and T_{ph} have been observed previously in [11].

Figs. 3a and 3b show T_{50} versus V_{DS} at 40 K and 300 K, respectively. The V_{GS} at each temperature were kept constant at the same values as for the S-parameter measurements. Similar trends of T_{50} with V_{DS} are observed at both T_{ph} , and the minimum value of T_{50} is reached at ~ 0.7 V. The measured T_{50} is determined by both the device minimum noise temperature and the mismatch (M_{sn}) between the optimum noise impedance (Z_{opt}) and 50 Ω . Understanding the observed T_{50} trends requires accounting for the M_{sn} or alternatively studying T_{min} which is independent of M_{sn} . T_{min} was determined using Keysight ADS once the SSM and noise models were established, and the result is plotted in Figs. 3a and 3b. T_{min} follows similar but less pronounced trends with V_{DS} as the measured T_{50} . The modelled M_{sn} is found to exhibit a weak dependence on V_{DS} for $V_{DS} < 0.8$ V and $T_{ph} = 300 \text{ K}$ and therefore cannot account fully for the trends of T_{50} with V_{DS} . The increase of T_{min} and T_{50} for $V_{DS} < 0.4$ V is explained by low g_m and high g_{ds} at low bias, while the increase for $V_{DS} > 0.6$ V is attributed to an increase in T_d with V_{DS} as discussed below. At $T_{ph} = 40$ K and $V_{DS} \ge 0.7$ V, the rise in T_{50} is attributed to M_{sn} .

In Fig. 3c, the T_{50} and modeled T_{min} are plotted at 6 GHz versus T_{ph} and $V_{DS}=0.6$ V, $I_{ds}=10$ mA. At this bias, both T_{50} and T_{min} exhibit weak dependence on T_{ph} for $T_{ph}\lesssim 100$ K, while at higher T_{ph} they increase linearly. Similar trends of T_{50} have been observed previously for GaAs mHEMTs [13] and InP pHEMTs [19].

Figs. 4a and 4b show the extracted T_d versus V_{DS} at T_{ph} of 40 K and 300 K, respectively. The T_d were extracted by fitting the modeled and measured T_{50} and therefore account for M_{sn} . Reference [1] modelled drain noise as the sum of a thermal and RST component:

$$T_d = T_{el} + T_{RST}(T_{el}) \tag{1}$$

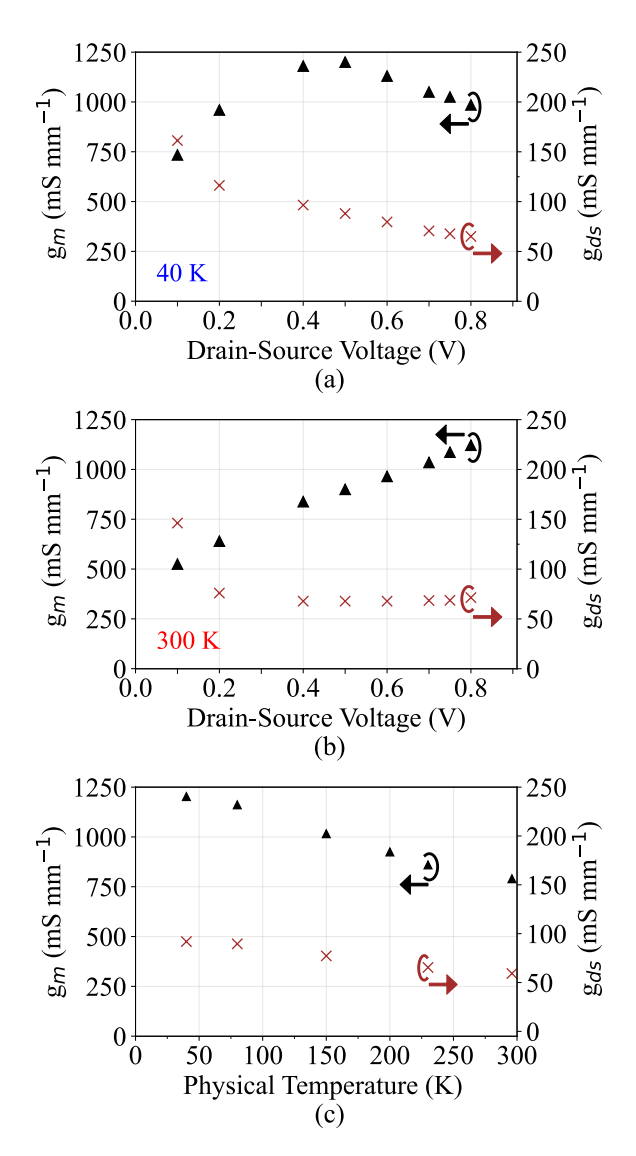


Fig. 2. Small signal g_m (y-left axis) and g_{ds} (y-right axis) versus V_{DS} at T_{ph} of 40 K (a) and 300 K (b). g_m and g_{ds} versus T_{ph} is shown in (c) at $V_{DS}=0.6$ V and $I_{DS}=10$ mA.

where $T_{RST}(T_{el}) \propto \exp\left[-(\Delta E_c - q(V_{GS} - V_{th}))/k_B T_{el}\right]$, with ΔE_c the conduction band offset, q the electric charge and k_B the Boltzmann constant. Given the extracted T_d , the solution of (1) at each V_{DS} yields T_{el} . We perform this calculation to determine T_{el} and T_{RST} at each V_{DS} and T_{ph} ; the results are shown in Figs. 4a and 4b. T_{el} rises with increasing V_{DS} ; however, the rate of increase is reduced once T_{el} reaches ~ 750 K. Similar trends of thermal noise in the channel with V_{DS} have been observed in [20]. The T_{RST} is small but a contributing part of T_d for $V_{DS} \lesssim 0.4$ V, while the rapid increase of T_{RST} at higher voltages indicates that RST becomes significant noise mechanism accounting for ~ 40 % and $\sim 70\%$ of T_d at $V_{DS} = 0.8$ V and 40 K and 300 K, respectively. The gate leakage currents remained below -0.5 $\mu A/\mathrm{mm}$ at all $V_{DS}\lesssim0.8~\mathrm{V}$ and therefore shot noise was not contributing factor in T_d . Additionally, S_{22}

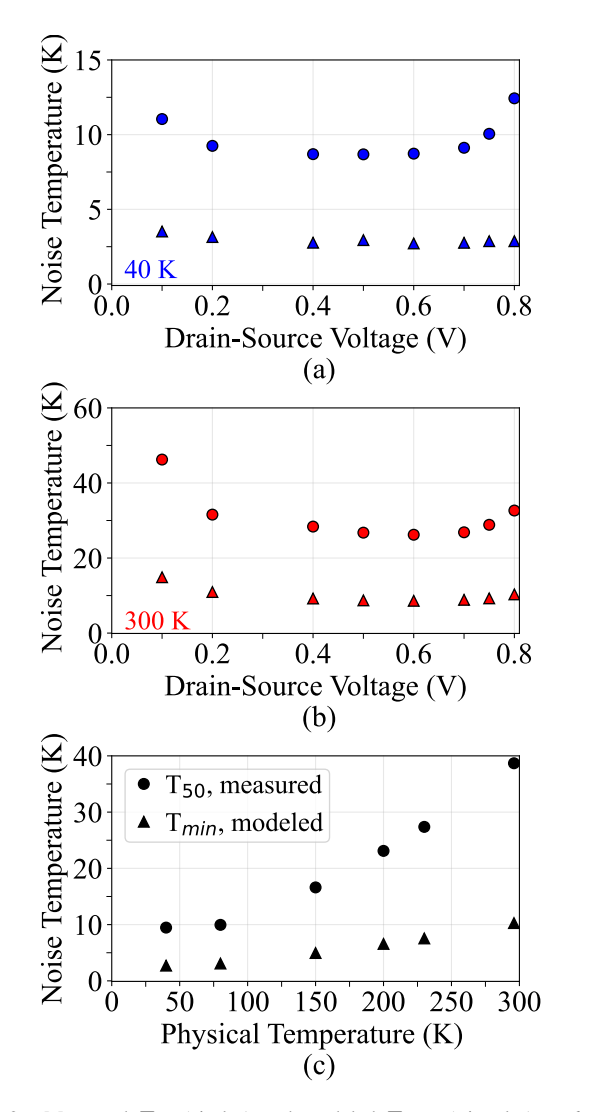


Fig. 3. Measured T_{50} (circles) and modeled T_{min} (triangles) at 6 GHz, versus V_{DS} at T_{ph} of 40 K (a) and 300 K (b) and constant V_{GS} of 12.9 mV and -10 mV, respectively, and versus T_{ph} (c) at constant $V_{DS}=0.6$ V and $I_{DS}=10$ mA.

remained capacitive [21] for all $V_{DS} < 0.8$ V while the output conductance did not show any hump for $V_{DS} < 0.8$ V [22], suggesting that impact ionization effects could be neglected. Fig. 4c shows the drain noise current power spectrum density (i_{dn}) as a function of T_{ph} at constant $V_{DS} = 0.6$ V and $I_{DS} = 10$ mA. A rise of i_{dn} with T_{ph} is consistent with previous reports [11], [1]. At $V_{DS} = 0.6$ V and $I_{DS} = 10$ mA, the M_{sn} does not vary with T_{ph} , and therefore the rise of T_{50} and T_{min} with increasing T_{ph} is driven by i_{dn} .

IV. DISCUSSION

We have found that the T_{50} of InP pHEMTs varies non-linearly with V_{DS} and T_{ph} , and that these trends cannot be explained by variations in mismatch with these parameters. Instead, the observations can be explained by an output drain noise power that varies with V_{DS} and T_{ph} . These dependencies are inconsistent with the predictions of the suppressed shot

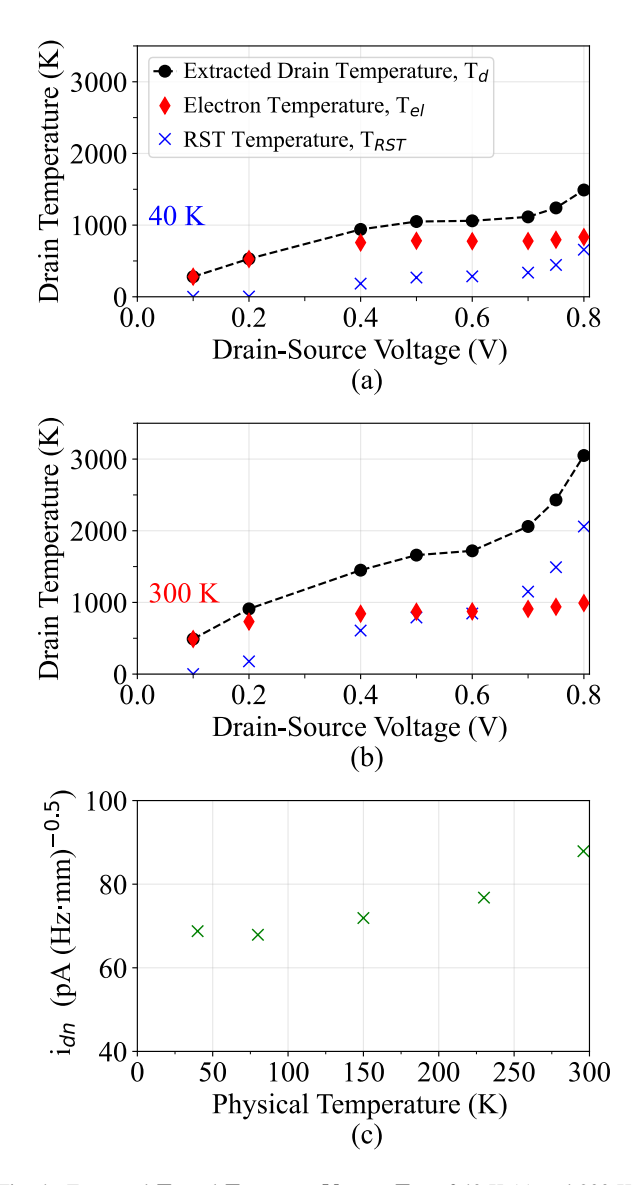


Fig. 4. Extracted T_d and T_{el} versus V_{DS} at T_{ph} of 40 K (a) and 300 K (b). T_{el} is derived from the extracted T_d based on [1, (1)]. The drain noise current spectral power versus T_{ph} is shown in (c) at $V_{DS}=0.6$ V, $I_{DS}=10$ mA.

noise theory but can be accounted for by the findings of [1] in which T_d was attributed to thermal and RST contributions.

In that work, the study of T_d in GaAs mHEMTs indicated that RST was negligible at $T_{ph}\lesssim 100$ K, while it accounted for over 50% of T_d at T_{ph} of 300 K. The observed trends of T_d with V_{DS} in the present work are in qualitative agreement with [1]. However, there are notable differences: the T_d of InP pHEMTs (Figs. 4a, 4b) rise with increasing V_{DS} and plateau for V_{DS} between ~ 0.4 V and ~ 0.6 V, followed by rapid increase at higher V_{DS} . In comparison the T_d for GaAs mHEMTs[1] rise gradually with V_{DS} . Additionally, at $T_{ph}=300$ K and $V_{DS}<0.8$ V, T_d takes smaller values for InP pHEMTs, varying from $\sim 500-\sim 3000$ K, compared to $\sim 700-\sim 3500$ K for GaAs mHEMTs. The lack of available data regarding the channel and barrier composition

of the devices complicates the interpretation and comparison of the results in terms of the RST process at present.

Finally, we discuss possible improvements to T_{min} which could be achieved if RST noise were suppressed. Replacing T_d with T_{el} in our noise model indicates that T_{min} would improve by $\sim 15\%$ at 40 K and $\sim 25\%$ at 300 K and $V_{DS}=0.6$ V. Our study sets the stage for future work in which the effect of quantum confinement on drain noise is systematically explored.

V. CONCLUSION

We have investigated the on-wafer microwave noise T_{50} and S-parameters of InP pHEMTs over a range of V_{DS} and T_{ph} . From these data, we have extracted T_d at each V_{DS} and T_{ph} , allowing for the noise mismatch at the various conditions to be accounted for using the noise model. We observed that T_d exhibited nonlinear trends with V_{DS} and T_{ph} which agree qualitatively with reported trends of T_d for GaAs mHEMTs [1]. The results support a recently proposed model of drain noise where T_d originates from the sum of thermal and RST noise. We modeled the effect of the suppression of the RST component of T_d on T_{min} and found that an improvement of $\sim 25\%$ in T_{min} at room temperature can be expected if RST noise were suppressed, e.g. by improved quantum well confinement.

ACKNOWLEDGMENT

This work was supported by the National Science Foundation under Grant No. 1911220.

REFERENCES

- B. Gabritchidze, K. Cleary, A. C. Readhead, and A. J. Minnich, "A physical model for drain noise in high electron mobility transistors: Theory and experiment," arxiv.org/abs/2209.02858.
- [2] I. Esho, A. Y. Choi, and A. J. Minnich, "Theory of drain noise in high electron mobility transistors based on real-space transfer," vol. 131, no. 8, 2022.
- [3] E. Cha, N. Wadefalk, G. Moschetti, A. Pourkabirian et al., "A 300-μw cryogenic hemt lna for quantum computing," in 2020 IEEE/MTT-S International Microwave Symposium (IMS), Aug. 2020, pp. 358–360.
- [4] B. Aja Abelan, M. Seelmann-Eggebert, D. Bruch, A. Leuther et al., "4–12 and 25–34 GHz cryogenic mhemt MMIC low-noise amplifiers," *IEEE Transactions on Microwave Theory and Techniques*, vol. 60, no. 12, pp. 4080–4088, 2012.
- [5] J. Schleen, G. Alestig, J. Halonen, A. Malmros et al., "Ultralow-power cryogenic inp hemt with minimum noise temperature of 1 k at 6 ghz," *IEEE Electron Device Letters*, vol. 33, no. 5, pp. 664–666, 2012.
- [6] F. Heinz, F. Thome, A. Leuther, and O. Ambacher, "A 50 nm gate-length metamorphic hemt technology optimized for cryogenic ultra-low-noise operation," *IEEE Transactions on Microwave Theory and Techniques*, vol. 69, no. 8, pp. 3896–3907, 2021.
- [7] S. Lorene, "An overview of solid-state integrated circuit amplifiers in the submillimeter-wave and thz regime," *IEEE Transactions on Terahertz Science and Technology*, vol. 1, no. 1, pp. 9–24, 2011.
- [8] S. Qu, X. Wang, C. Zhang, and Z. Wang, "6-7 GHz cryogenic low-noise mhemt-based amplifier for quantum computing," in 2019 Cross Strait Quad-Regional Radio Science and Wireless Technology Conference (CSQRWC), Jul. 2019, pp. 1 – 3.
- [9] F. Thome, F. Schafer, S. Turk, P. Yagoubov et al., "A 67–116 ghz cryogenic low-noise amplifier in a 50 nm InGaAs metamorphic hemt technology," *IEEE Microwave and Wireless Components Letters*, vol. 32, no. 5, pp. 430–433, 2022.
- [10] M. Pospieszalski, "On the limits of noise performance of field effect transistors," in 2017 IEEE MTT-S International Microwave Symposium (IMS), 2017, pp. 1953–1956.

- [11] F. Heinz, F. Thome, D. Schwantuschke, A. Leuther et al., "A scalable small-signal and noise model for high-electron-mobility transistors working down to cryogenic temperatures," *IEEE Transactions on Microwave Theory and Techniques*, vol. 70, no. 2, pp. 1097–1110, 2022.
- Microwave Theory and Techniques, vol. 70, no. 2, pp. 1097–1110, 2022.
 [12] R. Reuter, M. Agethen, U. Auer, S. van Waasen et al., "Investigation and modeling of impact ionization with regard to the rf and noise behavior of hfet," IEEE Transactions on Microwave Theory and Techniques, vol. 45, no. 6, pp. 977–983, 1997.
- [13] B. Gabritchidze, K. Cleary, J. Kooi, I. Esho et al., "Experimental characterization of temperature-dependent microwave noise of discrete hemts: Drain noise and real-space transfer," in 2022 IEEE/MTT-S International Microwave Symposium - IMS 2022, 2022, pp. 615–618.
- [14] A. R. Alt, D. Marti, and C. Bolognesi, "Transistor modeling: Robust small-signal equivalent circuit extraction in various hemt technologies," *IEEE Microwave Magazine*, vol. 14, no. 4, pp. 83–101, 2013.
- [15] Keysight Technologies Inc, "Pathwave advanced design system (ads)." [Online]. Available: www.keysight.com/
- [16] G. Kompa, Parameter Extraction and Complex Nonlinear Models. Norwood MA: Artech House, 2020.
- [17] E. Cha, N. Wadefalk, P.-A. Nilsson, J. Schleeh et al., "0.3—14 and 16—28 GHz wide-bandwidth cryogenic MMIC low-noise amplifiers," *IEEE Transactions on Microwave Theory and Techniques*, vol. 66, no. 11, pp. 4860–4869, 2018.
- [18] W. Sander and S. Jun, "Low noise amplifier with 7 K noise at 1.4 GHz and 25 c," *IEEE Transactions on Microwave Theory and Techniques*, vol. 69, no. 4, pp. 2345–2351, 2021.
- [19] M. A. McCulloch, J. Grahn, S. J. Melhuish, P.-A. Nilsson et al., "Dependence of noise temperature on physical temperature for cryogenic low-noise amplifiers," vol. 3, no. 1, p. 014003.
- [20] H. Wang, Y. Liu, K. Radhakrishnan, and G. I. Ng, "High frequency drain noise in inalas/ingaas/inp high electron mobility transistors in impact ionization regime," in 2006 International Conference on Indium Phosphide and Related Materials Conference Proceedings, 2006, pp. 36–38.
- [21] D. C. Ruiz, T. Saranovac, D. Han, O. Ostinelli et al., "Impact ionization control in 50 nm low-noise high-speed inp hemts with inas channel insets," in 2019 IEEE International Electron Devices Meeting (IEDM), 2019, pp. 9.3.1–9.3.4.
- [22] C.-Y. Chang, H.-T. Hsu, E. Y. Chang, C.-I. Kuo et al., "Investigation of impact ionization in inas-channel hemt for high-speed and low-power applications," *IEEE Electron Device Letters*, vol. 28, no. 10, pp. 856–858, 2007.